Design of the guide-vanes of an axial self-rectifying air-turbine for wave energy converters.

João Rodrigo dos Santos Ferreira Nunes
joao.ferreira.nunes@ist.utl.pt

Instituto Superior Técnico, Universidade de Lisboa, Portugal

June 2017

Abstract

The Oscillating Water Column is undoubtedly one of the most frequent operating principles in wave energy converters. In order to increase the efficiency and the operating range of these devices, self-rectifying turbines are used. These have two sets of guide vanes in their constitution, arranged symmetrically in relation to the rotor, avoiding the use of valves to rectify the reciprocating flow, thus making the system independent of the flow direction. The aim of this work is to dimension a set of guide vanes to integrate an axial self-rectifying impulse turbine. Due to the misalignment of the second stator, located downstream of the rotor, with the outflow, characteristic of a fixed blade configuration, a two-dimensional optimization is then performed in order to minimize these losses, improving the turbine's performance. Hence, a methodology is presented for the design of the guide vanes, attempting to mitigate this problem without neglecting the rotor's entry requirements. In addition to the optimization, unsteady state calculations are performed, due to the massive separations of the flow in the downstream stator, in order to validate the performance of the different configurations. Finally, a three-dimensional study of the guide vanes is carried out, evaluating the implication that the complex phenomena inherent to a three-dimensional flow will have in the final configuration, allowing to validate the methodology followed in this work, as well as to verify the performance of different possible configurations.

Keywords: Wave energy, Oscillating Water Column, Self-rectifying axial turbine, Design of guide vanes, Differential Evolution.

1. Introduction

The oscillating water column (OWC) is, undoubtedly, the most interesting operating principle in wave energy, being the one that has been more extensively studied and which presents a greater number of installed and operational mechanisms. These can be coupled with several types of turbines, being the self-rectifying turbines the most suitable ones, actually. They present a very wide range of operation, being able to function when subjected to irregular flows, typical of the real operating environment.

Self-rectifying turbines include two sets of guide-vanes, upstream and downstream of the rotor, the latter being responsible for a lower efficiency of the turbine. Since the first stator guides the flow upstream of the rotor, its symmetric ends up being misaligned with the exit flow, downstream of the rotor, providing a considerable separation of the fluid, causing significant stagnation pressure losses. To this phenomenon, wakes of significant dimensions are associated, with periodic release of vortices, inducing undesired vibrations in the structure complemented with high noise levels. In addition to this misalignment, that can never be mitigated in a fixed guide-vanes configuration, the blockage of the outlet is of the utmost importance, since a greater obstruction of the flow will lead to a greater loss of stagnation pressure, as it would be expected.

Different approaches in the development of a set of guide vanes were analyzed, but one of them stood out, not only for the concept itself, which *a priori* seemed promising, but mainly by its proved quality, supported by experimental results. In 2009, the Portuguese company *Kymaner*, within the *ModOndas* project [1], presented a stator consisting of two consecutive rows of guide-vanes, dividing the deflection of the flow by two phases, as can be seen in Fig. 1. With this innovative idea, they were able to maintain the necessary deflection required by the rotor, allowing the reduction of flow blockage at the outlet, since the integrating blades of this new stator have smaller dimensions (in the circumferential direction). Thus, the negative impact that the downstream stator has on the overall efficiency of the turbine was reduced.

Hence, the main focus of this project is to find a solution with a wide range of operation and good efficiency values, trying to meet these requirements with a simple and economical solution. A compromise between costs and efficiency is achieved by opting for an axial self-rectifying turbine that will perform better than a Wells turbine but will have lower manufacturing costs compared to a bi-radial turbine. In order to evaluate the performance of the set of guide-vanes designed, the turbine will have in its constitution the rotor used in the project CORES [2] which, at the time, operated with movable guide-vanes.

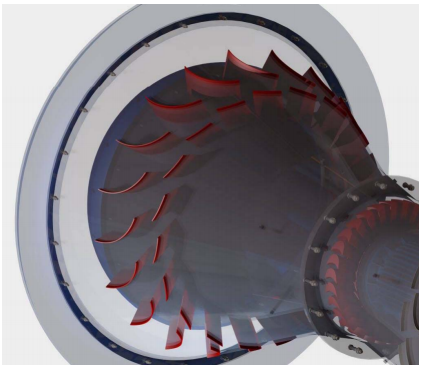

Figure 1: Stator of the axial self-rectifying impulse turbine developed by *Kymaner*, reproduced from [1].

Therefore, the main objective of this dissertation is to dimension the fixed guide-vanes of an axial self-rectifying impulse turbine, increasing their reliability and reducing their costs of manufacture and maintenance. The number of rows that will be present in each set of guide-vanes will be studied. The turbine's compactness is another design requirement so no diffuser will be dimensioned, which would bring benefits if added to the system. Further information on the CORES program and the turbine used can be found in [3].

A methodology capable of creating different two-dimensional geometries in a straightforward way is developed, which can be used by a genetic optimization algorithm (*Differential Evolution*, [4]), generating various blade profiles. The aerodynamic performance of each profile is then assessed with to a CFD software, allowing the algorithm to, through the use of genetic operations, improve the geometry, iteratively. Afterwards, the outflow is modeled, using time-dependent calculations, since the downstream stator can be regarded as a set of bluff-bodies, creating an unsteady flow. Different configurations will be tested in order to improve the stator's performance. To validate the followed methodology, the optimized guide-vanes are also modeled three-dimensionally, allowing to verify its performance in real conditions, especially, to ascertain the influence of different phenomena that emerge when the flow is confined.

2. Guide-vanes design

The design of the guide-vanes should be efficient and straightforward since thousands of evaluations will occur during the optimization. Therefore, it is necessary to generate the most diversified blade profiles possible using few variables to define them. More parameters will widen the spectrum of tested profiles, however, it will delay the convergence of the optimization. Taking this into consideration, Bézier curves are used to define the camber line of the profile, since they require few points, thus reducing the number of variables involved. The camber line is formed using 4 control points, corresponding 2 of them to the leading edge (LE) and the trailing edge (TE) of the blade, respectively. The position of the remaining control points will dictate the geometry of the camber line, making it more or less curved. The positioning of these two control points is always done in relation to the other two, which occupy the endpoints of the curve, as can be seen in Fig. 2.

Trying to reduce the number of variables involved, the position of these 2 points will be, in some way, limited. The control points lie on an arc of circumference (fixed radius), being the only variable the angle that the line joining the two points makes with the chord, Fig. 2. Thus, the distance between the second and the first control point, in a straight line, will always be the same. This is also true for the third and fourth control point, with the peculiarity that the distance may and will be different: $r_{\mathrm{LE}} = 0{,}4c$ and $r_{\mathrm{TE}} = 0{,}2c$, corresponding c to the chord. These values are the outcome of a preliminary study of the implications of the quantities used. They were chosen considering that they confer enough diversity to the generated camber lines. The profile's thickness is scaled from a NACA 63A012 [5], defining a scale factor to be optimized.

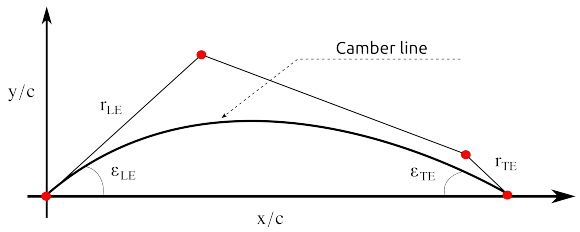

Figure 2: Bézier curve with 4 control points, 2 of them fixed.

The operation of the turbine's rotor requires an inlet flow in a certain direction, which can only be obtained with the use of guide-vanes. Thus,

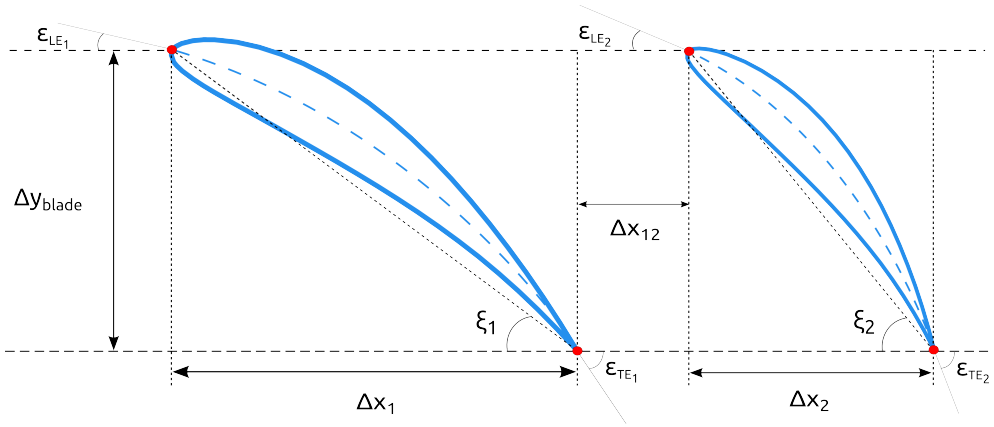

Figure 3: Blades parameters for a two guide-vane stator.

the strategy is to partition the flow deflection into stages. Basically, achieve the desired deflection by imposing the air to flow through several rows of guide-vanes. This seeks a reduction in the ratio between the circumferential length of the blades (Δy_{blade}) and the pitch by decreasing the blockage of the outflow. This reduction of the geometric blockage is only achieved taking advantage of the "shadow" effect provided by the first row of guide-vanes (facing the flow downstream of the rotor). Thus, it is necessary to clarify what is the geometric blockage factor, which is defined as the ratio between the length Δy_{blade} and the pitch (the circumferential distance between two consecutive blades), given in percentage by

$$\psi\,(\%) = \frac{\Delta y_{\text{blade}}}{\Delta\Theta} \times 100\% \tag{1}$$

where $\Delta\Theta$, which varies through the span of the blade, is defined as

$$\Delta\Theta = \frac{2\pi r}{Z_{\text{stator}}} \tag{2}$$

and Z_{stator} corresponds to the number of blades used in each row of the stator. This can be easily understood by analyzing Fig. 3, where it can be perceived that the 2 blades are perfectly aligned. The geometric blockage factor indicates the obstructed path of the flow exiting the rotor and is associated with the pressure losses of the turbine, as it will be seen further in this document.

With the imposition of a certain blockage factor a vertical length of the blade, y_{blade} is obtained. Therefore, it is still necessary to define a length in the perpendicular direction, x, with respect to the leading edge, where the trailing edge of the blade is situated. This length will be one of the optimization parameters. Having the location of the two ends of the blade defined, it is possible to position it in space, being this method used for all the blades that constitute the stator, Fig. 3. The leading edge of the first blade is fixed in the computational domain in order to obtain a reference coordinate, from which the rest of the points are defined. This approach permits to easily determine the chord of the profile and its stagger angle, ξ. To sum up, all the optimization parameters can be summarized in Table 1, where 2 rows were used as an example, being the other cases, 3 or more, analogous.

Table 1: Optimization parameters for 2 rows of guide vanes

ϵ_{LE_1}, ϵ_{LE_2}	angles of the leading edge
ϵ_{TE_1}, ϵ_{TE_2}	angles of the trailing edge
s_1, s_2	thickness factors
Δx_1, Δx_2	axial lengths
Δx_{12}	distance between blades

Finally, since the blades will have a stagger angle different of 90°, the wake generated by them is prone to be deflected in a preferential direction. Therefore, a relative rotation between the rows of guide vanes will be done trying to minimize the pressure losses of the second stator. This displacement λ, defined in Eq. 3, corresponds to the vertical distance that separates the leading edges of the two blades, and can be positive, if $y_{LE_2} > y_{LE_1}$ or negative if the opposite happens. A value of λ null corresponds to the initial situation, with aligned blades. This quantity λ will be nondimensionalized by Δy_{blade}.

$$\lambda = \frac{y_{LE_2} - y_{LE_1}}{\Delta_{y_{blade}}} \tag{3}$$

Considering the dimensions of the turbine used it is necessary to take into account that to a large amount of guide-vanes will correspond blades with a high aspect ratio, which will be expensive to manufacture if it is ensured that the blades offer the necessary structural resistance without induc-

ing undesirable vibrations in the flow, compromising the stator's performance. On the other hand, a reduced number of guide-vanes will lead to weaker flow guidance and a higher presence of secondary flows caused by more pronounced pressure gradients. Therefore, it is again necessary to establish a compromise between these two extremes, trying to avoid the harmful effects of each one of them. Since it is not possible to analyze the presence of secondary flows in a two-dimensional analysis (nor is it feasible to do a three-dimensional analysis in an initial phase), the number of guide-vanes to be used was determined by checking if its aspect ratio would be the most appropriate for the problem. In conclusion, it was obtained $Z_{\text{stator}} = 23$, which is the value used in the following phases of this work.

3. Mesh generation

To evaluate the performance of the different geometries generated, a computational mesh has to be generated. A hybrid mesh was chosen, since it can be constituted by different kinds of blocks, satisfying the requirements of each area of the domain, see Fig. 4.

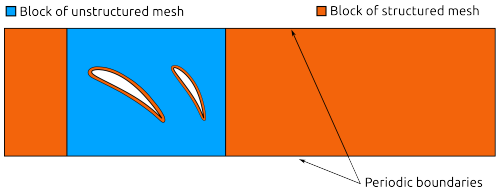

Figure 4: Computational domain.

It presents blocks of structured mesh at the inlet and outlet of the domain because they practically remain constant during all evaluations being, this way, more efficient. The other structured blocks correspond to the "O" mesh, contiguous with the surface of the blades. These ones present a set of consecutive layers, increasing its dimensions exponentially, allowing to generate really small elements near the surface, to verify the requirement of $y^+ < 1$. On the outer end of the block, a proper bonding with the other mesh block is guaranteed by having elements of similar dimensions. The surface presents a non-linear distribution of points, avoiding the generation of defective elements (too wide) in the regions of high-curvature where strong gradients are expected (trailing edge), generating a more refined mesh in this area see Fig. 5.

The remaining domain, corresponding to the area surrounding the blades, displays an unstructured mesh, generated based on Delaunay [6] triangulations. It is versatile, enabling a proper adaptation of the mesh to the different countours of the blades created, connecting the upstream and the downstream blocks. The cohesion of all this blocks in

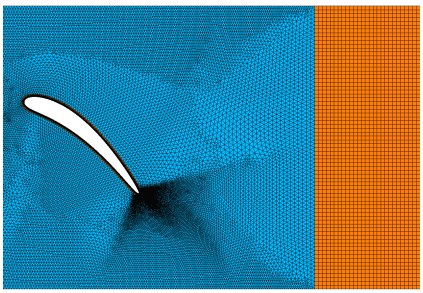

Figure 5: Cohesion of the different mesh blocks.

ensured by using the same point distribution at the borders of adjacent blocks. The computational domain is then delimited externally by 4 borders: an inlet, an outlet and 2 periodic boundaries which reduces the time consumed by each calculation, see Fig. 4. To calculate the outflow, the computational domain used is practically the same, just changing the dimensions of the upstream and downstream blocks, since the wake is, in this case located on the opposite side of the blades.

4. Optimization

Taking into consideration the nature of the problem, the main characteristics that the guide-vanes must present are easily identified: a correct deflection of the flow and a low (minimum possible) pressure drop. Thus, the objective function of this optimization could be to combine these two variables by measuring the absolute angle of the flow at the input of the rotor (output of the first stator) and the stagnation pressure drop through the stator. However, using two variables that are intrinsically different from each other, a weight factor would have to be applied. This ponderation would be challenging since there is no correct value to use and different ones would lead to different results.

Therefore, this multi-objective optimization can be partitioned into two stages, where the pressure losses are evaluated by the boundary layer's separation, excluding the results which do not verify certain requirements [5]. If the flow does not separate until a defined length of the suction side, the respective geometry is then accepted by the algorithm, analyzing its flow deflection.

$$F(z) = \alpha_2 \tag{4}$$

However, taking into account what has already been presented before, pressure losses are much more relevant in the second stator and are proportional to the flow blockage, ψ. Thus, it could be expected that this variable was included in the objective function trying to minimize it. However, the blockage factor affects the value of the angle of the flow proportionally, in other words, a greater fac-

tor corresponds to a greater deflection. This dependence makes it impossible to conjugate the two variables. Hence, and considering what is intended, a value of ψ is defined *a priori* for each optimization, comparing the optimized geometry's performance to the deflection required to that radius. The value of α_2 obtained (within an acceptance range) is analyzed and the process is repeated with a more suitable ψ if the result is not satisfactory. It is a time-consuming iterative process that is facilitated by the use of a genetic algorithm of optimization (DE) that allows to provide a certain geometry as input, ensuring that the best results are used in the following optimizations. The algorithm offers a wide range of options, being the */best* scheme used, since it converges more rapidly, which is important due to the significant number of optimizations that are performed. Therefore, the single-term objective function is quite simple, being defined in Eq. 4.

5. Numerical model

The relevant details regarding the numerical model will be here presented, as well as the operating conditions of the turbine and the rotor's requirements.

5.1. Operating conditions

The Table 2 summarizes the geometric characteristics of the rotor, corresponding Λ to the height of the channel.

Table 2: Geometric characteristics of the rotor

Z_{rotor}	r_{tip}[m]	r_{mean}[m]	r_{hub}[m]	Λ[m]
31	1.0	0.86798	0.678	0.322

Considering the angles of relative velocity at the 3 given sections [2] and using the design condition of $V_{2\text{t}} = 2U$, being $\Omega = 180\,\text{rpm}$, the desired flow deflection α_2 was obtained, presented in table 3 where r^* is defined as $r^* = (r - r_{\text{hub}})/(r_{\text{tip}} - r_{\text{hub}})$.

Table 3: Angles of absolute velocity upstream the rotor

r^*	0.00	0.59	1.00
α_2^* [°]	43.73	46.87	47.46

The axial velocity of the inlet flow is $V_a = 34{,}927\,\text{m/s}$ which considering the dimensions of the channel leads to volumetric flow rate of $Q = 59{,}29\,\text{m}^3/\text{s}$. The working fluid is air at ambient temperature ($T_{\text{amb}} = 300\,\text{K}$) with $\rho = 1{,}225\,\text{kg/m}^3$ and a dynamic viscosity of $\mu = 1.7894\,\text{Pa.s}$.

5.2. Flow computation

The numerical simulation of the inlet flow requires the imposition of a few boundary conditions which correspond to certain restrictions at the boundaries of the computational domain. These must be carefully chosen so that the simulation does not develop in an erroneous way, providing unrealistic results. In order to better describe the inlet flow it was necessary to provide more characteristic details of a turbulent flow. Thus, a turbulent intensity value of 5% and a turbulent viscosity ratio of 10, corresponding to typical values for this range of Reynolds numbers (approximately 2.0×10^5), were assigned to characterize turbulence intensity. At the outlet, the *outflow* condition was chosen, commonly used when pressure and velocity values are unknown *a priori* [7]. A no-slip boundary condition was imposed to the blade surfaces. Periodicity conditions were also applied, useful in the study of axissymmetric problems. In this way, the two periodic boundaries (see Fig. 4) are associated, minimizing the computational effort inherent to these calculations.

They were carried out using a commercial software, *Fluent*, solving the Reynolds-Averaged Navier-Stokes equations (RANS) with a $\kappa - \omega$ SST turbulence model. A viscous, turbulent, incompressible ($\text{Ma} < 0.3$ at ambient temperature) and steady-state flow was assumed. The equations were solved employing a pressure-based solver (coupled) using a second order scheme for the pressure equation and second order upwind schemes for the other ones.

The outflow conditions are assumed to be unsteady due to the massive flow separation occurring when the flow reaches the second stator. In this situation, a time-dependent calculation is performed which requires a temporal discretization of the equations. The boundary conditions are similar to the ones described before, presenting the inlet of the second stator the same axial velocity, since the cross-sectional area remains unchanged and a null tangential velocity is assumed at the exit of the rotor. The main difference resides at the turbulence characteristic values, since the passage of the flow through the stator has to be taken into account, increasing the intensity of the turbulent phenomena.

6. 2D Analysis

Blade profiles were optimized for the mid-section mentioned in Table 3, using 1, 2 and 3 rows of guide-vanes. Trying to reduce the blockage factor, more rows were introduced in the stator, still verifying the rotor requirements regarding the angle of the absolute velocity, α_2. Table 4 summarizes this first optimization, clearly indicating, as expected, that an increase of the number of rows minimizes

the blockage factor. The introduction of a second row drastically changes the value of ψ, although, adding a third row does not improve much. It can be concluded that this strategy follows an asymptotic trend, presenting, at a certain point, a stagnation of the value of ψ, independently of how many rows are added.

Number of rows (Z_c)	1	2	3
ψ [%]	42.00	29.10	23.00
$F(z)$ [°]	46.99	46.87	47.05

Table 4: Optimization for design angle $\alpha_2^* = 46.87\,°$, for $r^* = 0{,}59$.

This analysis simplifies the optimization process, so it is not necessary to optimize the 3 sections of the three configurations, significantly reducing the time spent in obtaining the profiles that allow generating the guiding-vanes that will constitute the stator. Then, the performance of these different configurations was analyzed, obtaining the stagnation pressure drop (Δp_0) verified in each one of them, for various Reynolds numbers. The Reynolds number was calculated using as reference length the circumferential chord of the blades, Δy_{blade}, see (Eq.5).

$$\text{Re}_{\text{stator}} = \frac{V_{\text{a}} \Delta y_{\text{blade}}}{\nu} \tag{5}$$

Thus, a dimensionless coefficient of the stagnation pressure drop, $K_{\text{p}_{\text{outlet}}}$,is defined, where Δp_0 is the stagnation pressure drop across the second stator and V_a is the velocity at the output of the rotor.

$$K_{\text{p}_{\text{outlet}}} = \frac{\Delta p_0}{\frac{1}{2}\rho V_a^2}, \tag{6}$$

In Fig.6 the variation of this dimensionless parameter with the Reynolds number is represented.

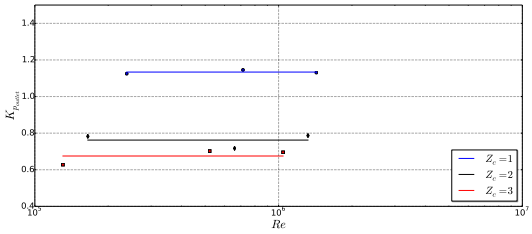

Figure 6: Pressure losses for different configurations.

It is thus proved that the followed approach is advantageous, as well as the expected interdependence between the geometric blockage and the losses in the second stator. In short, it can be stated that the addition of a third row does not present itself as the best alternative, since the gain, namely the decrease of this dimensionless pressure coefficient, is not significant, not offering great improvements in the performance of this stator and implying higher manufacturing costs as well as greater complexity of the overall system. In addition, it is also important to highlight the independence of the losses with the Reynolds number, derived from the massive flow separation, resulting in a large turbulent wake.

Having defined the number of rows to use ($Z_c = 2$), the remaining sections were optimized. The results of this first optimization showed a few problematic characteristics. To start with, a negative angle of the LE of the first blade was verified, creating a highly curved profile which can originate a recirculation bubble in its pressure side when subject to real conditions. Moreover, the profiles were quite different between them, regarding their dimensions. The preponderance of the first profile in the stator was evident and, therefore, subject to a significantly higher aerodynamic loading, not evenly dividing the flow between the two rows. This is not advantageous since a severely loaded blade is more prone to boundary layer separation due to the adverse pressure gradients present. Therefore, a few constraints were introduced in the optimization, trying to mitigate this deficiencies and enabling the generation of more regular blades. It is also important to mention that the other 2 sections optimized were drawn away from the hub and shroud of the turbine, since secondary flows are present in this areas, compromising the performance of the optimized sections. The new dimensionless radius chosen were $r^* = 0{,}15$ and $r^* = 0{,}85$, being the new respective design angles obtained by interpolating the values present in Table 3 with a quadratic function.

Once obtained the final configuration, the relative rotation between the rows was considered, being the main analysis carried out for the mid-section followed by the study of its implications in the remaining sections of the blade. In this way, a misalignment between the two rows was imposed, trying to follow the deflection of the wake originated by the first blade facing the outflow. Thus, following what was described previously, several tests were carried out for different rotations, by ascertaining the impact of the different blade arrangements on the losses of the second stator. The Fig. 7 shows the variation of the dimensionless coefficient of pressure losses as a function of the imposed offset.

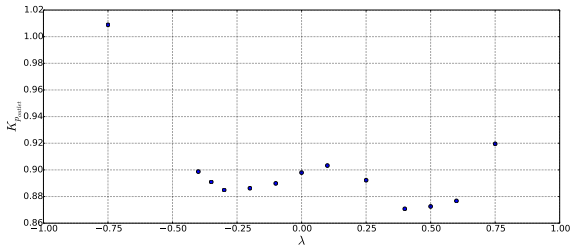

Figure 7: Pressure losses for different offsets, λ.

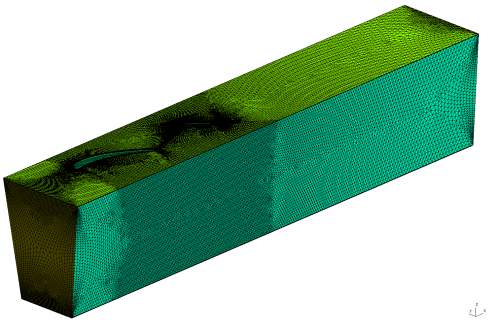

Figure 8: 3D mesh, composed by different blocks.

Positive and negative offsets were tested for a minimum value of $K_{p_{outlet}}$ in order to increase overall turbine's efficiency. The most extreme points, $\lambda = -0.75$ and $\lambda = 0.75$, validate the shadow effect since much higher pressure losses are verified compared to the remaining values. It should be noted that the obtained gains are marginal, never representing a great improvement in the performance of the second stator. Although, since these offsets do not imply an increase of the turbine's manufacturing costs or complexity, the best cases were tested, for $\lambda = -0.30$ and $\lambda = 0.40$. These were quite similar to the ones of the original case, in the shroud, with a sligh but acceptable difference of α_2. However, at the hub, the situation was completely different, where recirculating flow appeared at the pressure side of the second blade profile. This corresponds to an unstable situation that could easily diverge to a more significant flow separation, in real conditions. To sum up, the rotation of the rows did not contribute to an improvement of the stator's performance, being the final configuration chosen composed of perfectly aligned blades.

7. 3D analysis

The main focus of this analysis is to verify if the bidimensional optimization can be considered an adequate methodology to design the guide-vanes of an axial self-rectifying turbine.

7.1. Generation of the hybrid mesh

The computational mesh once again presented different blocks in its composition, being mostly composed of unstructured mesh, as can be seen in Fig. 8. The presence of structured mesh blocks is verified in the surrounding areas of the blades and it is essential to ensure the correct modeling of the boundary layer in this zone, again imposing the requirement of $y^+ < 1$ on the surface. This constraint is also applied to the remaining walls of the domain, namely the hub and shroud, whose zones are filled by individual mesh blocks, as will be illustrated later.

The initial phase consists of generating the meshes corresponding to the guide-vanes. They define the blade in space and are composed of hexahedrons. The elements contiguous to the surface of the blade are very small (10^{-6} m), increasing exponentially in the normal direction off the surface. This mesh block is constructed based on different layers, which are successively "stacked", see Fig. 9. However, due to the variation of the optimized blade profiles along the wingspan, these layers also have slight differences between them. This happens because the mesh has to follow the different profiles that the blade has along its wingspan. Thus, with only 3 sections of the blade being optimized at different radii, it was necessary to generate the intermediate profiles, to be used in each layer.

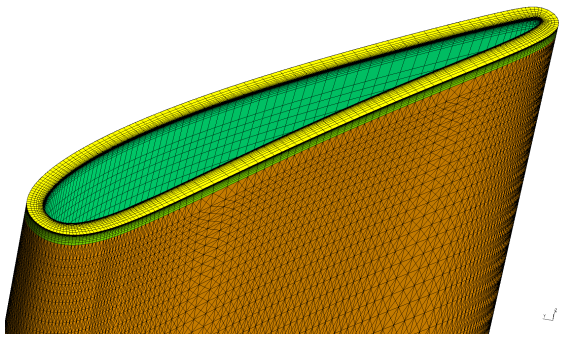

Figure 9: Blade's "O" mesh block.

The use of a quadratic interpolation was sufficient for the creation of the remaining profiles. The number of layers used was 137, which can be grouped in 25 for both the hub and shroud, as will be explained later, plus 89 for the intermediate zone of the domain. It should be noted that the last layer of the hub block corresponds to the first layer of the intermediate zone as the last layer of the layer corresponds to the first layer of the shroud block. The profile surface is discretized using 201 points, being the "O" mesh consisted of 25 elements in the normal direction to the surface.

Then, the mesh blocks corresponding to the hub

and shroud are generated, following the same approach. Fig. 10 represents a detail of the hub's mesh block, where the different layers used can be seen, increasing its height in an exponential way.

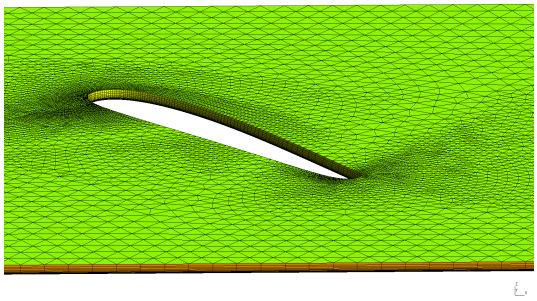

Figure 10: Hub's mesh block.

Identical to those generated in the two-dimensional case, once again the external contours of the domain as well as the contour that discretizes the profile associated with that radius, were defined. The same unstructured mesh generator is used to fill the domain according to the distribution of points presented by the contours. The main difference in this case is that these layers, significantly close together, are used to generate a three-dimensional mesh block. Basically, due to the reduced differences that the layers present between themselves and the smooth variation of the profiles along such small distances of the wingspan, it is possible to create triangular prismatic elements between layers, Fig. 11.

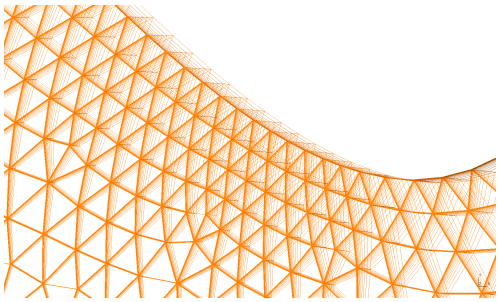

Figure 11: Hub's mesh block: detail of the TE.

It should be noted that, due to the small dimensions of the elements located at the TE area, the layers must be very close in order to avoid conflicts in the generation of the prismatic elements. So much closer depending on the variability of the blade along its wingspan. This is an important detail, since the last layers that constitute the mesh block already have a significant distance between them, being necessary to determine the most suitable parameters that allow a correct mesh generation.

In order to generate the main mesh block it is necessary to confine the domain of interest, defining the surfaces that delimit it. Thus, 4 more surfaces are generated, which can be seen as lateral surfaces. The approach followed is the same as the one presented in 2D: the outer contours are defined being the respective area filled with triangular elements. Two surfaces correspond to the inlet and outlet of the domain and the remaining two are the lateral surfaces, constituting the periodic boundaries. Having the volume of the computation domain delimited (4 lateral surfaces, hub's top layer, shroud's bottom layer and the blade's surfaces), it is filled with tetrahedral elements, using an unstructured mesh generator. The refinement of the main mesh block is controled with the respective refinement of the outer surfaces which define it.

7.2. Boundary conditions

The boundary conditions applied are practically the same with a small difference: a *Pressure Outlet* condition was now applied, activating the option of radial equilibrium at the outlet section. Atmospheric pressure is then imposed to the smaller radius, being the rest of the span calculated according to the radial equilibrium. A Green-Gauss node based gradient evaluation was chosen, being this averaging scheme more accurate than the default cell-based scheme for unstructured meshes, most notably for tetrahedral meshes [7], which corresponds to the majority of the computational domain.

7.3. Three-dimensional flow

The 3D flow is, intrinsically, much more difficult to calculate. The addition of the hub and shroud walls are responsible for an augmented complexity of the flow, being responsible for the presence of secondary flows near the walls. These lead to a poor performance of the guide-vanes at these regions, which can influence the flow at its core. A more detailed description of the nature of these flows can be found at [8].

7.4. Different 3D configurations

Previously, the approach followed for the construction of the blades was explained. However, this process has an important feature, which provides a greater multiplicity to this project. Although the optimized two-dimensional sections have a reference point that allows to relate all the lengths associated with the profiles, it does not correspond to the same position for the different sections. This enables the creation of various blades with the same optimization thus, not rejecting numerous other possible configurations. Therefore, several stators were analyzed, not being feasible to include this parameter in the 2D optimization. The sweep angle of the blades is the main characteristic that distinguishes

the different options studied. This variable plays an important role in the control of the harmful effects of the secondary flows [9]. In an intuitive way, five different configurations were defined, arranged in the following mode: centering the distance between TE_1 and LE_2 (A), centering the distance between LE_1 and TE_2 (B), centering the first blade (C), centering the second blade (D) or blocking the TE_2 (E).

7.5. Performance analysis

In order to evaluate the performance of the different stators, two quantities of interest were monitored: pressure drop and flow deflection. The pressure drop was calculated and is presented in its dimensionless form, K_p, in Table 5. It is verified that the values for each configuration are relatively identical, being concluded that this approach hardly contributes to the final choice, conferring greater importance to the second amount of interest.

Table 5: Values of K_p for the analysed configurations

Stator	A	B	C	D	E
K_p	2,024	2,024	2,022	2,023	2,014

Regarding the ascertainment of the flow deflection, a few cross-sectional areas were analysed, determining the values of α_2 along the span of the channel. Concerning the presentation of the results, a sum of the squared differences was chosen, Eq. 7, giving greater emphasis to the regions where there was a greater disparity between the design angle (α_2^*) and the calculated one (α_2). A total of 20% of the wingspan was ignored, 10% at each end, since it is considered that a good performance is not expected in these regions, thus not serving as a comparative element.

$$\sum_{i=0,1\Lambda}^{i=0,9\Lambda} (\alpha_{2_i}^* - \alpha_{2_i})^2 \tag{7}$$

However, the cross-section to use is yet to be defined, since a certain distance between the rotor and the stator was not required. It is recalled that the compactness of the turbine was one of the objectives of this project, trying to establish a balance between the performance of the turbine and its axial length. Six different cross sections were defined, 25 mm apart from each other, defining a minimum distance of 100 mm (corresponding to a maximum distance of 225 mm). This distance is measured from the point of the second blade closest to the rotor. The best results for each configuration are presented in Table 6.

It is easily seen that the first 4 configurations perform very similarly. It is recalled that, since a low variability of the profiles along the span was imposed, the configurations genereated were quite identical. As far as the rotor distance is concerned, it can be verified that in the best cases the minimum distance always corresponds to the best configuration. Since the wall zones exhibit significantly larger deflections than the rest of the domain, as can be seen in Fig. 12, a homogenization of the velocity profile occurs as the distance to the rotor increases, negatively affecting the deflection in the areas within the core domain.

Table 6: Summary of the best results for each stator and the respective distance to the rotor

Stator	$\sum_{i=0,1\Lambda}^{i=0,9\Lambda} (\alpha_{2_i}^* - \alpha_{2_i})^2$	Distance [mm]
A	3,1507	100
B	3,3204	100
C	3,3987	100
D	3,3587	100
E	5,0103	125

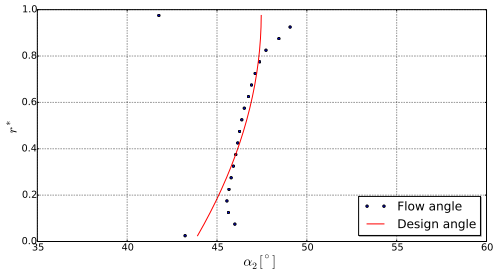

Figure 12: Distribution of the flow angle compared to the design one at a distance of 100 mm to the rotor (config. A).

It is also important to highlight that, considering 80% of the wingspan, percentage chosen in this evaluation, the distance to the rotor presented by the 4 best configurations always corresponded to the minimum distance, indicating that better configurations could be found with smaller distances. This situation was then verified considering two new distances, 70 mm and 80 mm. These have shown a better performance, albeit slight, and these new distances might not be the best choice, since larger disparities are found in the regions of the walls (which can compromise the performance of the rotor) increasing the probability of having, in real situations, a not fully developed flow at the entrance of the rotor.

To sum up, configuration A was the chosen one, presenting the best deflection of the flow, and a similar pressure drop to the other candidates. The distribution of α_2 for a distance of 100 mm to the rotor

is presented in Fig.12 and the final configuration can be seen in Fig. 13.

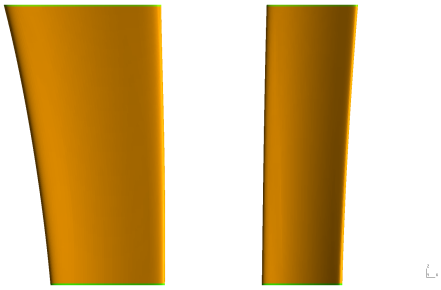

Figure 13: Side view of the optimized guide-vanes.

8. Conclusions

The methodology implemented in this dissertation was robust and versatile, allowing the generation of several systems of guide-vanes, both in the number of rows that constitute it and in the shape of the profiles used. The optimization based on the rotor operating conditions proved to be efficient, since the desired flow deflection was obtained, minimizing the geometric blockage created by the set of guide-vanes. Due to the misalignment of the flow with the second stator, efforts were made to attenuate its influence on the turbine's performance, trying to validate the methodology presented in [5]. The investigation of the behavior of the stator when subjected to the outflow of the rotor, with time-dependent calculations, was relevant in order to validate the above mentioned strategy of distributing the deflection by several aligned rows.

The three-dimensional mesh generation algorithm proved to be efficient and adequate to this project, since it allowed the creation of different boundary layer mesh blocks, with high control of its parameters, crucial considering the chosen turbulence model. Its robustness is also high, allowing the construction of three-dimensional meshes for the different numbers of rows tested and for numerous forms of blades, regardless of the variations verified along the wingspan. The three-dimensional modeling of the stator has proved to be essential. In this scheme, the flow has a significantly more intricate nature, with complex phenomena, especially in the endwalls, which are responsible for severe perturbations in the stator's operation.

In general, it can be concluded that the strategy followed was suitable, not only by the set of guide-vanes dimensioned that meets the operation requirements of the rotor, but also by the presented methodology. It is an expeditious and practical method, especially when compared to a three-dimensional optimization scheme, that allows the design of an axial turbine's stator.

In order to quantify the benefit which the adopted strategy has on the overall efficiency of the turbine, it is therefore important to calculate the flow combining the set of guide-vanes with the rotor for which they were dimensioned. Including, clearly, the second stator, this simulation would allow to obtain the turbine's operating curves, making it possible to establish the necessary comparison with the set of previously used movable guide-vanes. Finally, it is advisable to carry out experimental tests to validate the behavior of the optimized stator, analyzing the experimental pressure drop and the profile of α_2 obtained, according to the defined distance to the rotor.

References

[1] L. Trigo, "Kymaner presentation - The OWC option," `http://www.wavec.org/content/files/04_Luis_Trigo_Kymaner.pdf`. Accessed: 2017-05-08.

[2] R P F Gomes, J C C Henriques, L M C Gato, and A F O Falcão, Multi-point aerodynamic optimization of the rotor blade sections of an axial-flow impulse air turbine for wave energy conversion, *Energy*, 45(1):570–580, 2012.

[3] Cores, Components for Ocean Renewable Energy Systems (CORES) - Final Summary Report, *Eu Fp7 - 213633*, 2012.

[4] Rainer Storn and Kenneth Price, Differential evolution–a simple and efficient heuristic for global optimization over continuous spaces, *Journal of global optimization*, 11(4):341–359, 1997.

[5] André Maduro, Numerical optimization of the guide-vanes of a biradial self-rectifying air turbine, Master's thesis, IST - University of Lisbon, 2016.

[6] J.-D. Müller, P. L. Roe, and H. Deconinck, "A frontal approach for internal node generation in Delaunay triangulations," *International Journal for Numerical Methods in Fluids*, vol. 17, no. 3, pp. 241–255, 1993.

[7] Fluent-Inc, Fluent 6.3 Users Guide, *Fluent documentation*, 2006.

[8] Piotr Lampart, Investigation of Endwall Flows and Losses in, *Journal of Theoretical and Applied Mechanics*, 47(2):321–342, 2009.

[9] M A Neshat, M Akhlaghi, A Fathi, and H Khaledi, Investigating the effect of blade sweep and lean in one stage of an industrial gas turbine transonic compressor, *Propulsion and Power Research*, 4(4):221–229, 2015.